

SUPPLEMENTARY INFORMATION

Structure and efflux mechanism of the yeast pleiotropic drug resistance transporter Pdr5

Andrzej Harris¹, Manuel Wagner^{2,a}, Dijun Du^{1,b}, Stefanie Raschka², Lea-Marie Nentwig², Holger Gohlke^{3,4,5,6}, Sander H. J. Smits^{2,7}, Ben F. Luisi^{1*}, Lutz Schmitt^{2*}

¹: Department of Biochemistry, University of Cambridge, 80 Tennis Court Road, Cambridge, CB2 1GA, United Kingdom

²: Institute of Biochemistry, Heinrich Heine University Düsseldorf, Universitätsstraße 1, 40225 Düsseldorf, Germany

³: Institute of Pharmaceutical and Medicinal Pharmacy, Heinrich Heine University Düsseldorf, Universitätsstraße 1, 40225 Düsseldorf, Germany

⁴: John von Neumann Institute for Computing (NIC), Jülich Supercomputing Centre (JSC), Forschungszentrum Jülich GmbH, 52425 Jülich, Germany

⁵: Institute of Biological Information Processing (IBI-7: Structural Biochemistry), Forschungszentrum Jülich GmbH, 52425 Jülich, Germany

⁶: Institute of Bio- and Geosciences (IBG-4: Bioinformatics), Forschungszentrum Jülich GmbH, 52425 Jülich, Germany

⁷: Center for Structural Studies, Heinrich Heine University Düsseldorf, Universitätsstraße 1, 40225 Düsseldorf, Germany

^a: present address: Medac GmbH, Theaterstraße 6, 22880 Wedel, Germany

^b: present address: School of Life Sciences and Technology, ShanghaiTech University, 393 Middle Huaxia Road, Pudong, Shanghai, China

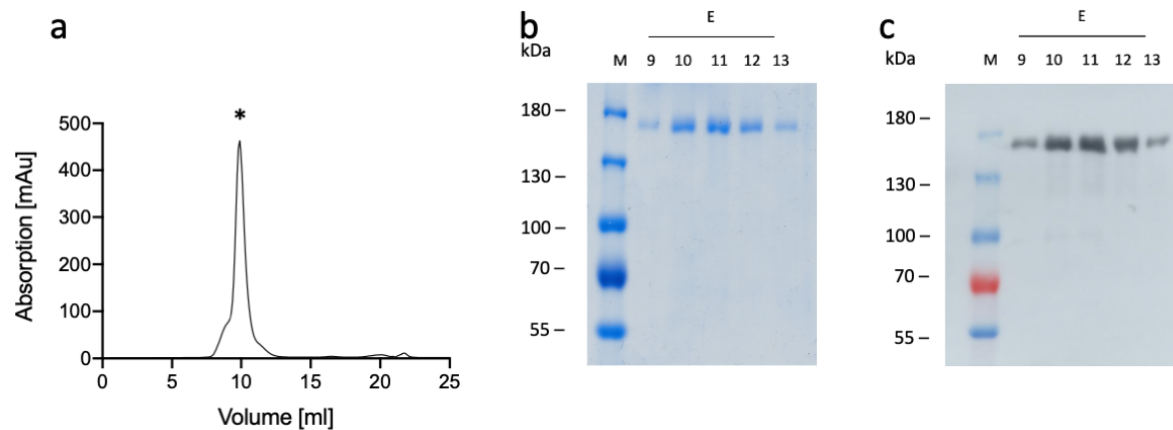
*: to whom correspondence should be addressed:

Ben F. Luisi
Department of Biochemistry
University of Cambridge
80 Tennis Court Road
Cambridge CB2 1GA, United Kingdom
phone: 00441223766029
email: bfl20@cam.ac.uk

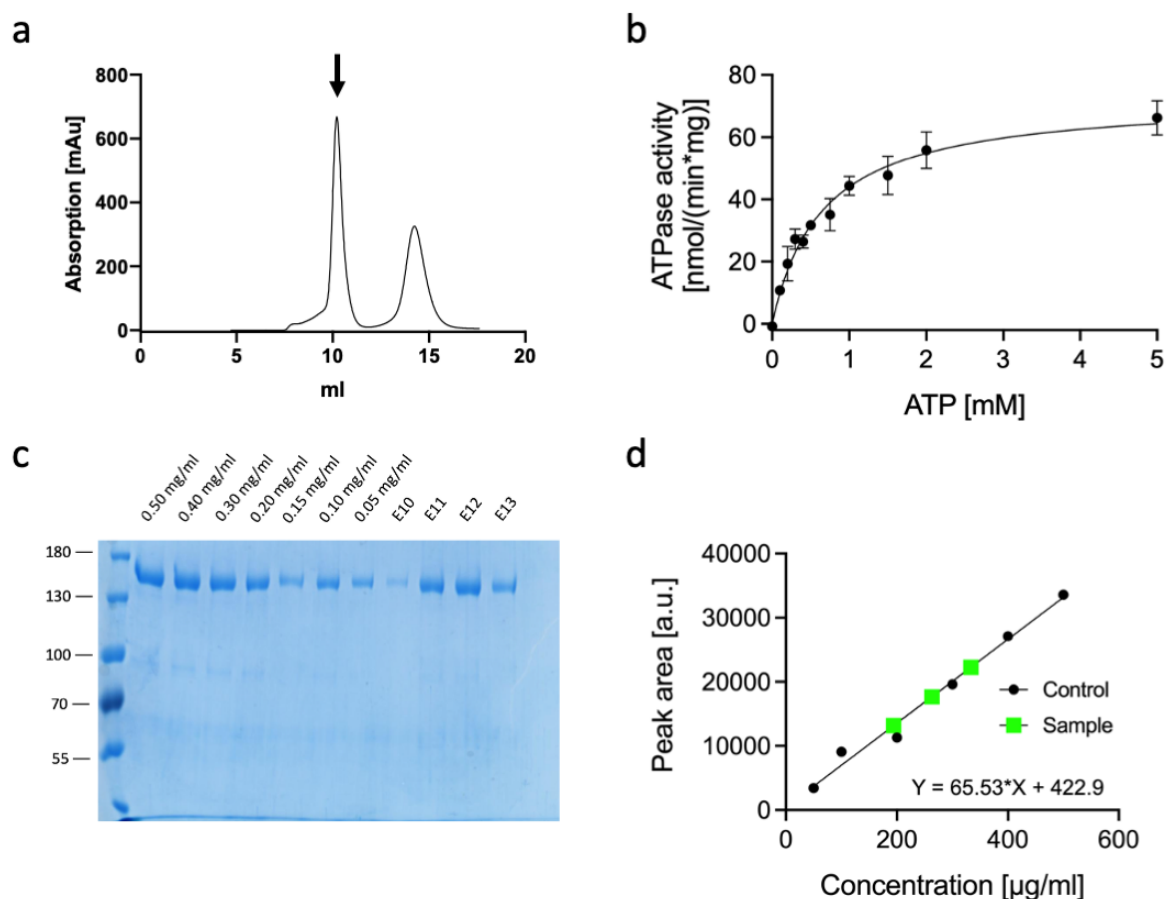
Lutz Schmitt
Institute of Biochemistry
Heinrich Heine University Düsseldorf
Universitätsstraße 1
40225 Düsseldorf, Germany
phone: 00492118110773
email: lutz.schmitt@hhu.de

These authors contributed equally: Andrzej Harris, Manuel Wagner, Dijun Du

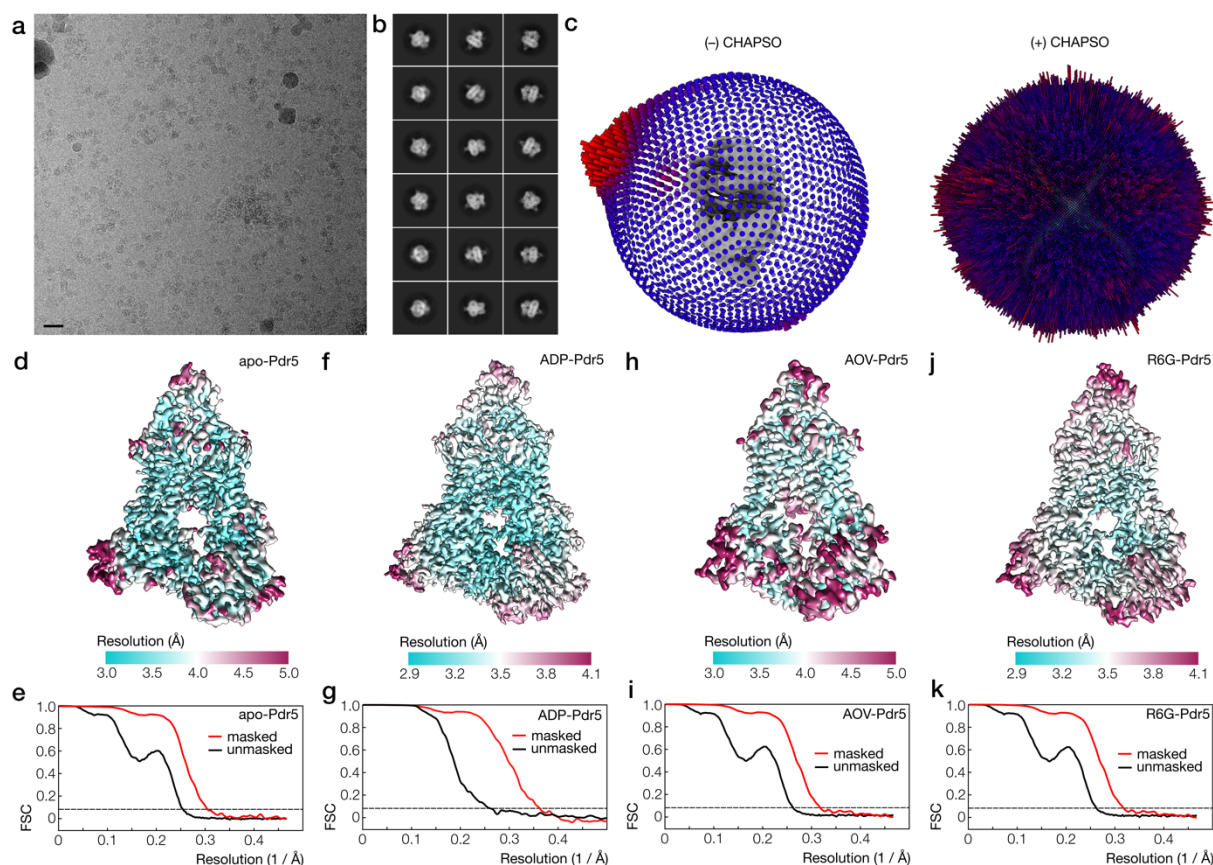
Supplementary Figures



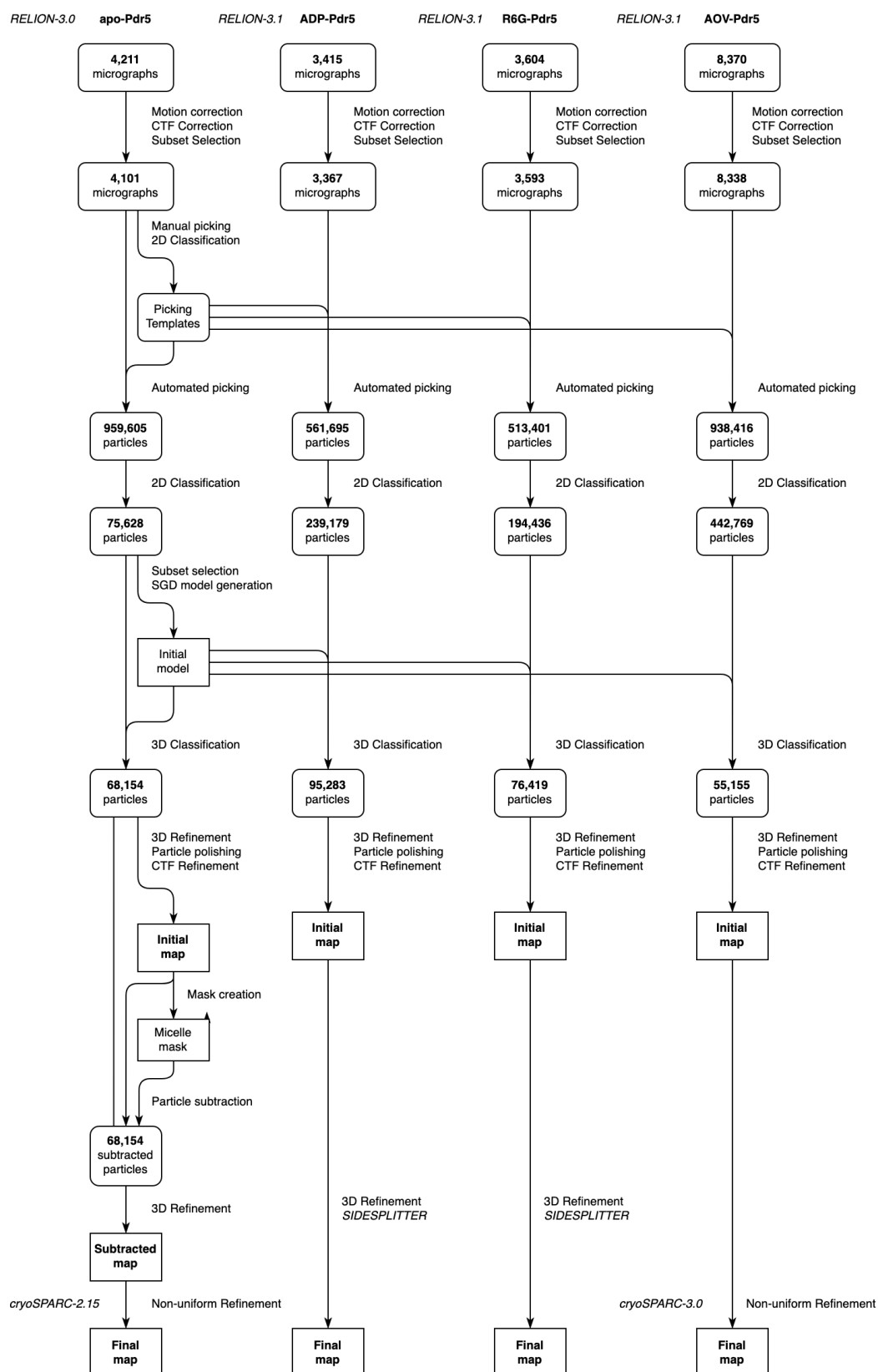
Supplementary Figure 1. Purification of Pdr5. **a** Size-exclusion chromatogram of Pdr5 solubilised in *trans*-PCC- α -M, as described in *Materials and Methods* section. Pdr5 elution is marked by an asterisk. **b** Coomassie-blue stained SDS-PAGE of purified Pdr5 (single repeat). **c** Western blot of the SDS-PAGE using a polyclonal Pdr5 antibody (single repeat). Molecular weight standards are given to the left of the SDS-PAGE and the Western blot. Source data are provided as a Source Data file.



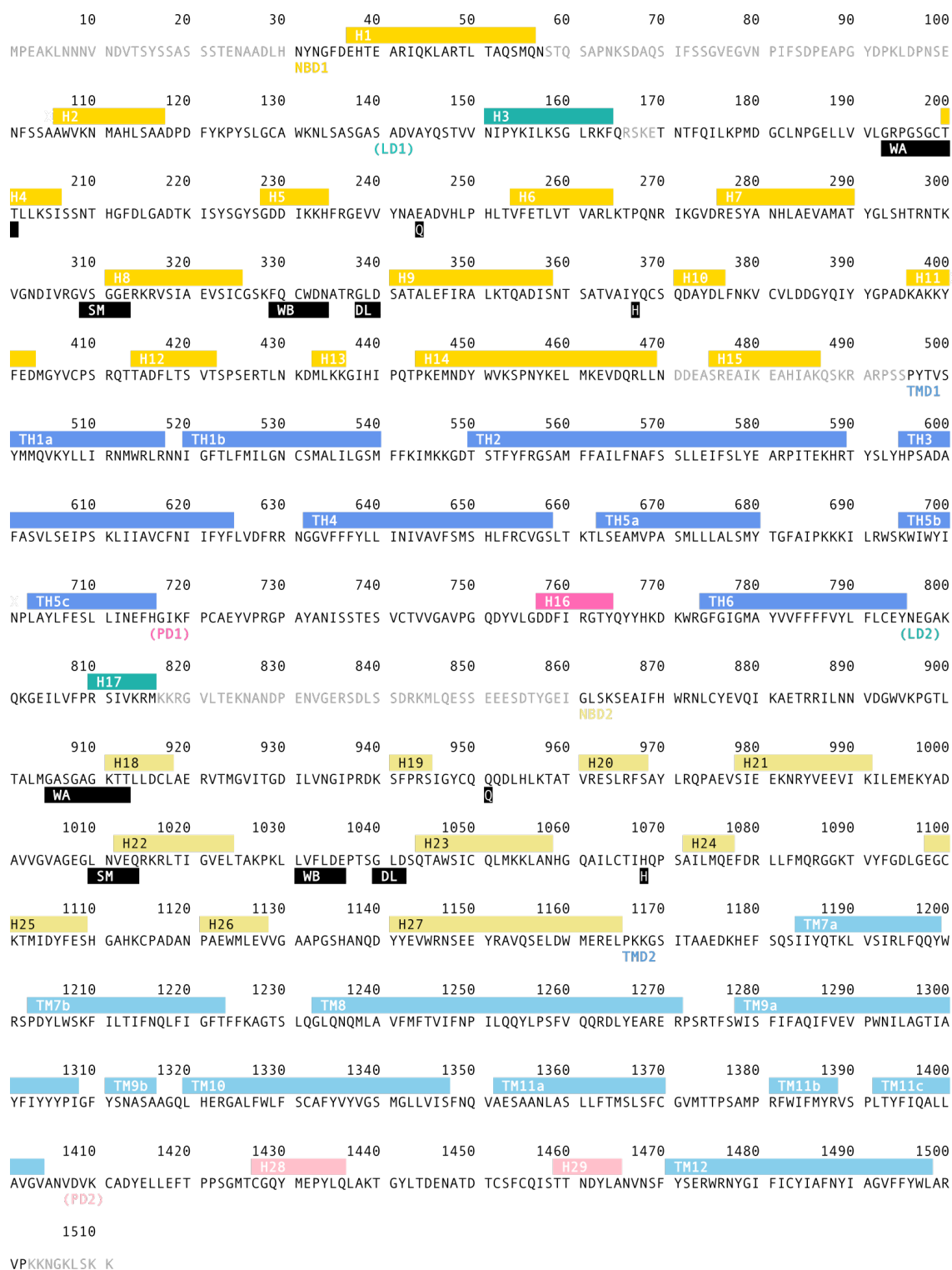
Supplementary Figure 2. Reconstitution of Pdr5 into peptidiscs. **a** Size-exclusion chromatogram of Pdr5 reconstituted into peptidisc, as described in *Materials and Methods* section. The peak of reconstituted Pdr5 is indicated by an arrow. **b** Pdr5 specific ATPase activity of reconstituted Pdr5. Error bars present mean \pm standard error of three independent experiments. **c** Coomassie-blue stained SDS-PAGE of Pdr5 samples of known concentration and elution fractions of the reconstitution experiment (single repeat). **d** Calibration line of the samples of Pdr5 of known concentration (black circles) and the three elution fractions of the reconstitution experiment (green squares, E11 to E13 from left to right). The equation of the linear regression is also provided. Source data are provided as a Source Data file.



Supplementary Figure 3. Cryo-EM imaging of Pdr5. **a** Cryo-EM micrograph (selected from a set of 3,415) of Pdr5/peptidisc particles in vitrified ice (ADP-Pdr5 sample). Scale bar is 300 Å. **b** Averaged images of the particles, obtained in reference-free 2D classification. **c** Angular distribution of particle orientations in Pdr5 samples prepared with and without the addition of CHAPSO. **d** Cryo-EM map of apo-Pdr5, coloured by local resolution (see key). **e** Gold-standard FSC curves showing the correlation between the half-datasets in the unmasked (black line) and masked (red line) maps. The overall resolution was judged using the $FSC_{0.143}$ threshold (dashed line). **f–k** Cryo-EM maps and FSC curves for the other Pdr5 reconstruction, analogous to **d–e**. See also: Supplementary Table 1. Abbreviations: FSC, Fourier-shell correlation.

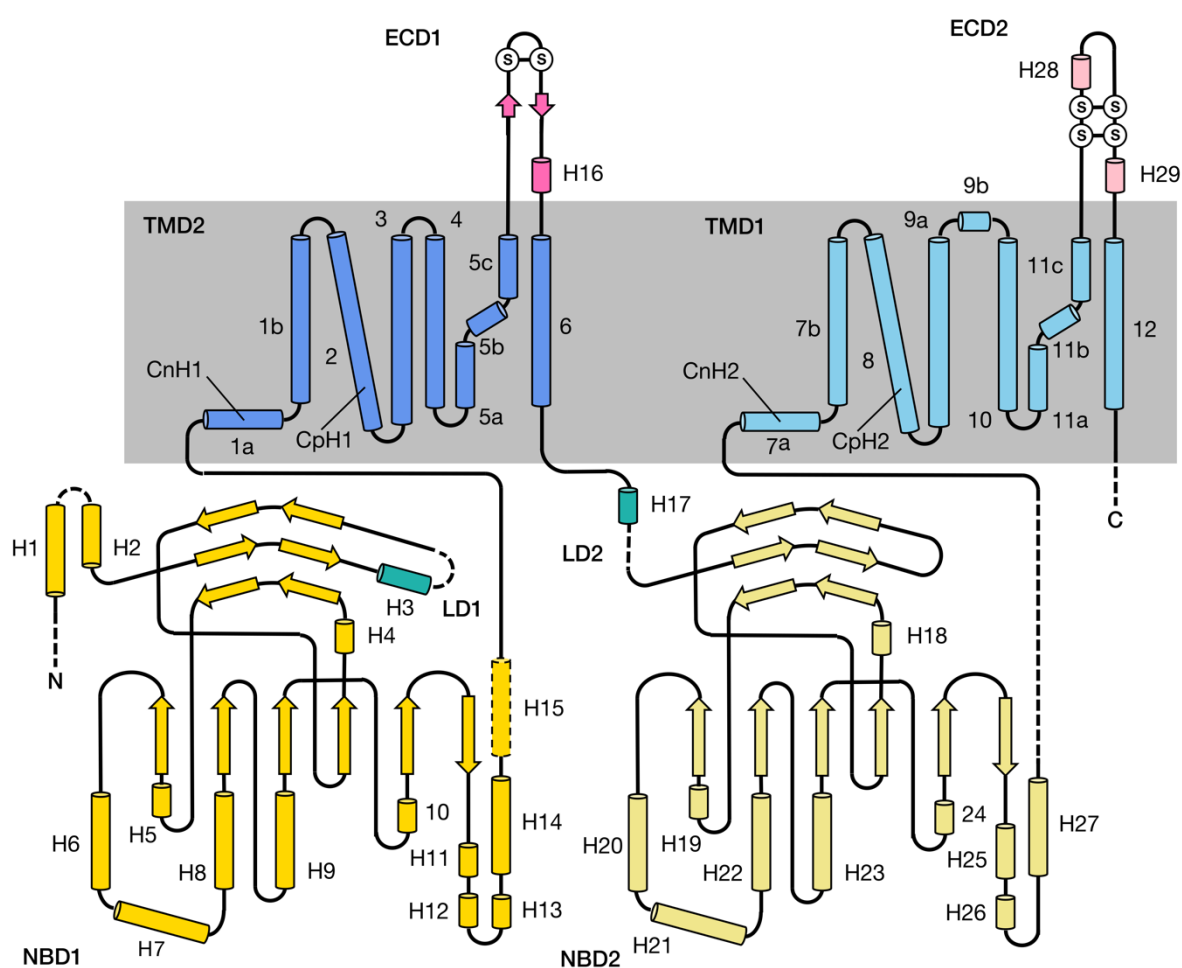


Supplementary Figure 4. Cryo-EM processing workflow for Pdr5 datasets. The diagram depicts schematically the steps in the computational analysis of the cryo-EM datasets that were collected in this study and used to reconstruct the four Pdr5 maps: apo-Pdr5, ADP-Pdr5, R6G-Pdr5 and AOV-Pdr5. Software packages, programs and individual procedures are listed, together with micrograph and particle numbers. Additional information is found in *Materials and Methods* section.



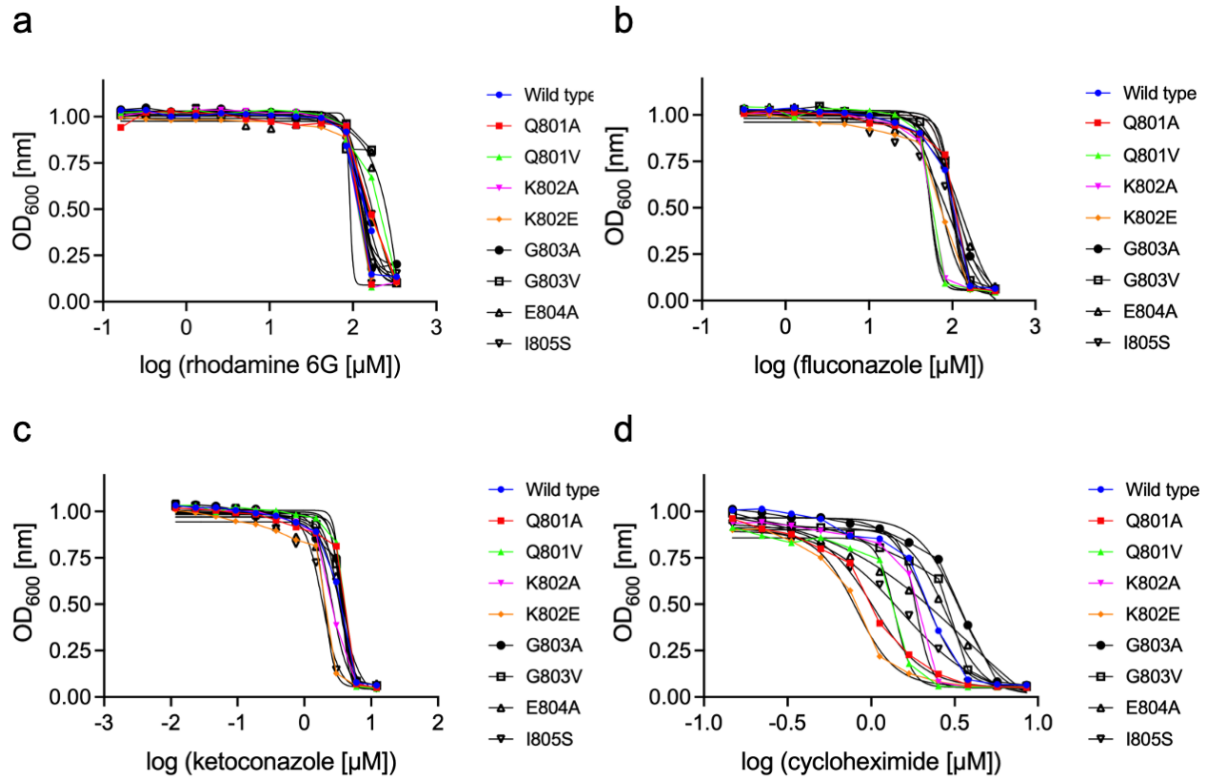
Supplementary Figure 5. Annotated amino-acid sequence of Pdr5. Indicated are conserved features of the nucleotide binding sites (black boxes) and positions of α -helices (coloured boxes). The domains of Pdr5 are indicated, and the helices are coloured according to the scheme used elsewhere in the paper. Grey residues indicate parts of the ADP-Pdr5 model that could not be resolved in the cryo-EM map.

Abbreviations: DL, D-loop; ECD, extracellular domain; H, H-loop; LD, linker domain; NBD, nucleotide-binding domain; Q, Q-loop; SM, signature motif; TH, transmembrane helix; TMD, transmembrane domain; WA, Walker A (or P-loop); WB, Walker B (or A-loop).

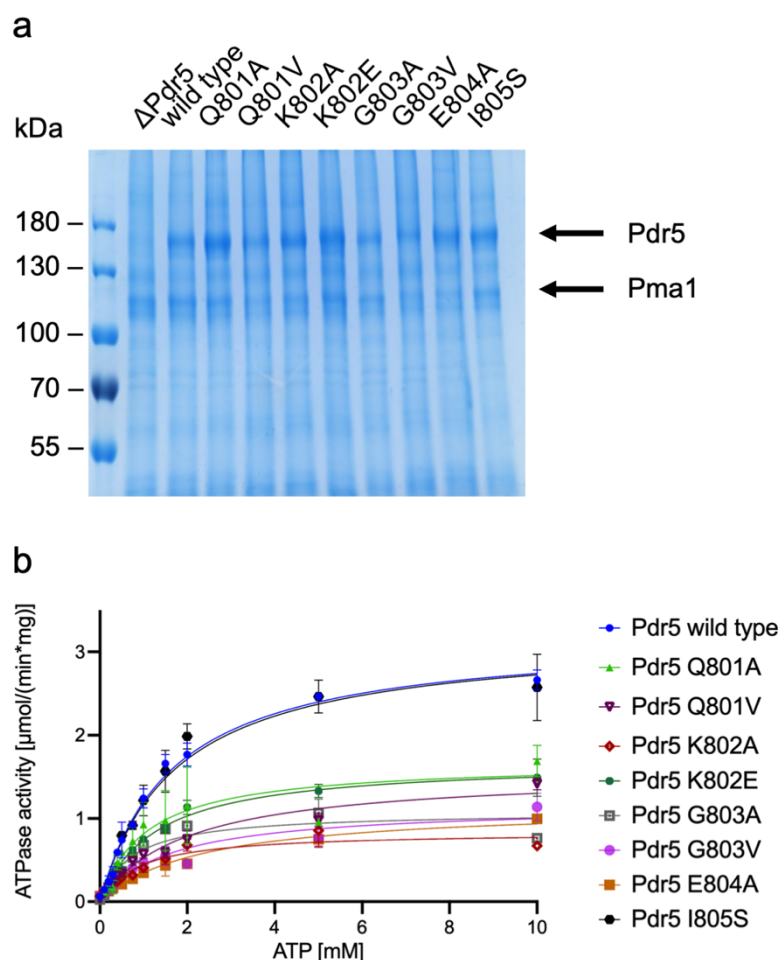


Supplementary Figure 6. Domain topology of Pdr5. A schematic representation of domain architecture of Pdr5 showing the arrangement of its secondary structural elements. Cylinders and arrows represent alpha-helices and beta-sheets. The elements on the diagram are not shown to scale, but their relative positioning in the two halves of the protein reflects the evolutionary relation of the transporter domains through a gene-duplication event. The colour scheme for domains is similar to the one used elsewhere in text. The dashed lines represent structure fragments that could not be resolved in the ADP-Pdr5 map (*cf.* Supplementary Figure 5). The circled letters “S” denote the position of disulphide bridges. According to the alternative nomenclature proposed for the PDR family¹, ECD1 and ECD2 are respectively EC3 and EC6.

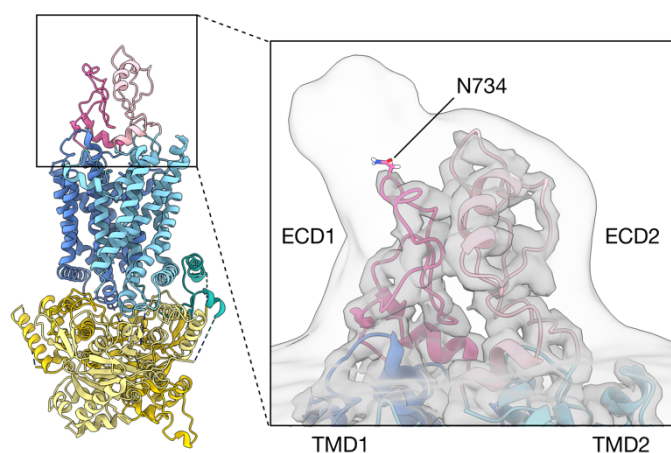
Abbreviations: ECD, extracellular domain; LD, linker domain; NBD, nucleotide-binding domain; TMD, transmembrane domain.



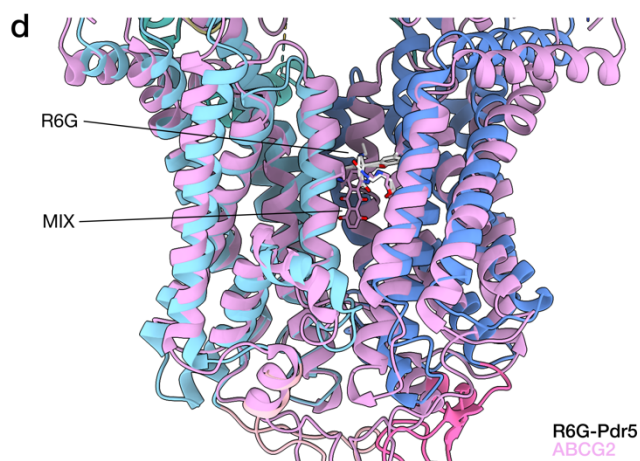
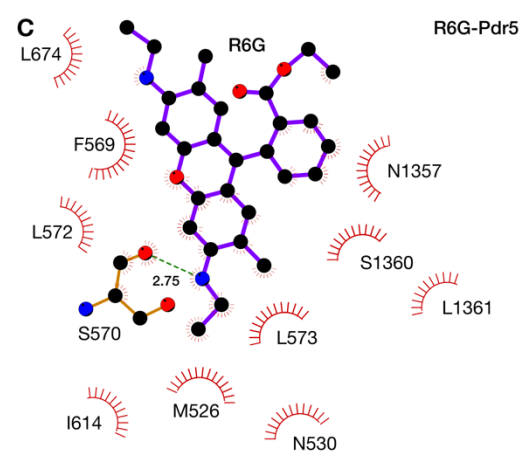
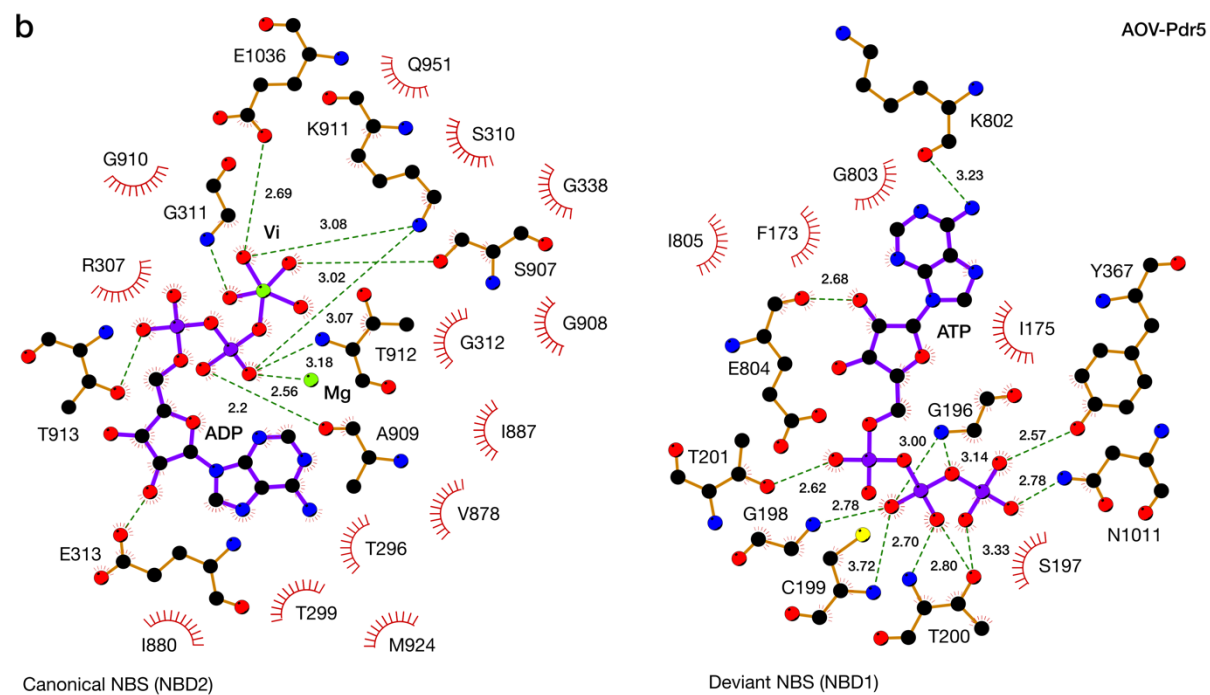
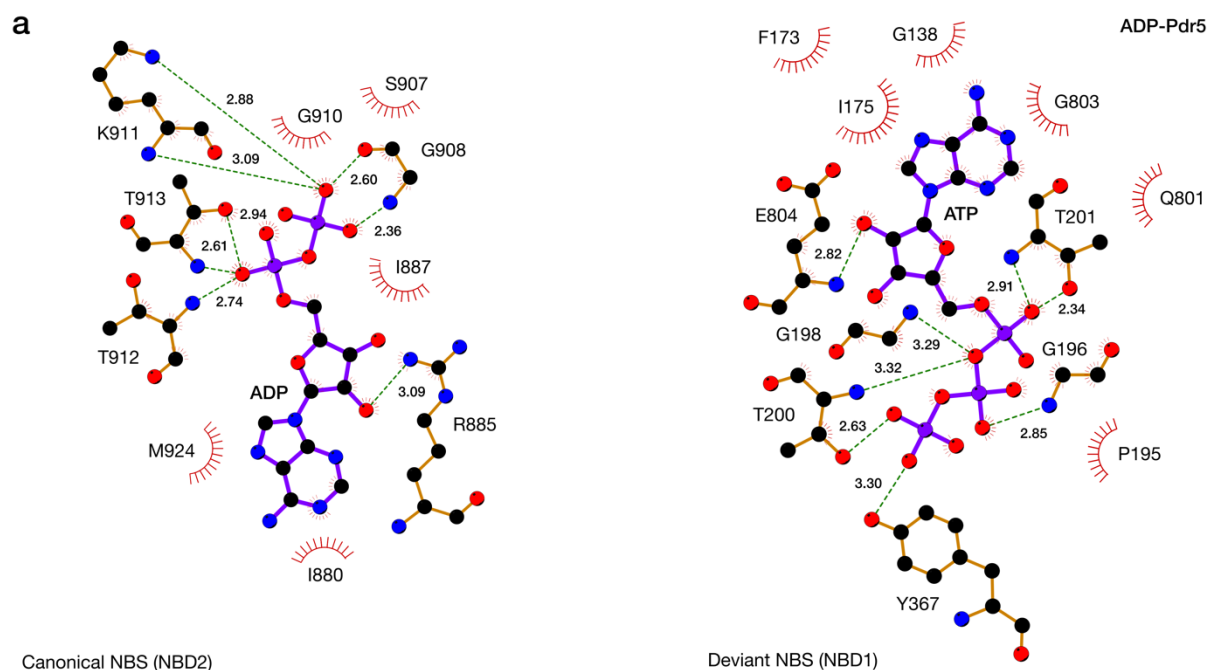
Supplementary Figure 7. Liquid drug assay for Pdr5 linker domain mutants. Yeast cells expressing Pdr5 (blue) or mutants in the linker domain (LD) were incubated for 48 hours at 30 °C with four different drugs at indicated concentrations. Subsequently, optical density at 600 nm (OD₆₀₀) was measured. Data were analysed using a log (inhibitor) vs response function implemented in Prism 9 (GraphPad Inc.). Experimental details of the assay are provided in the Methods section. The drugs investigated were **a** R6G, **b** fluconazole, **c** ketoconazole, and **d** cycloheximide. See also: Supplementary Table 3.



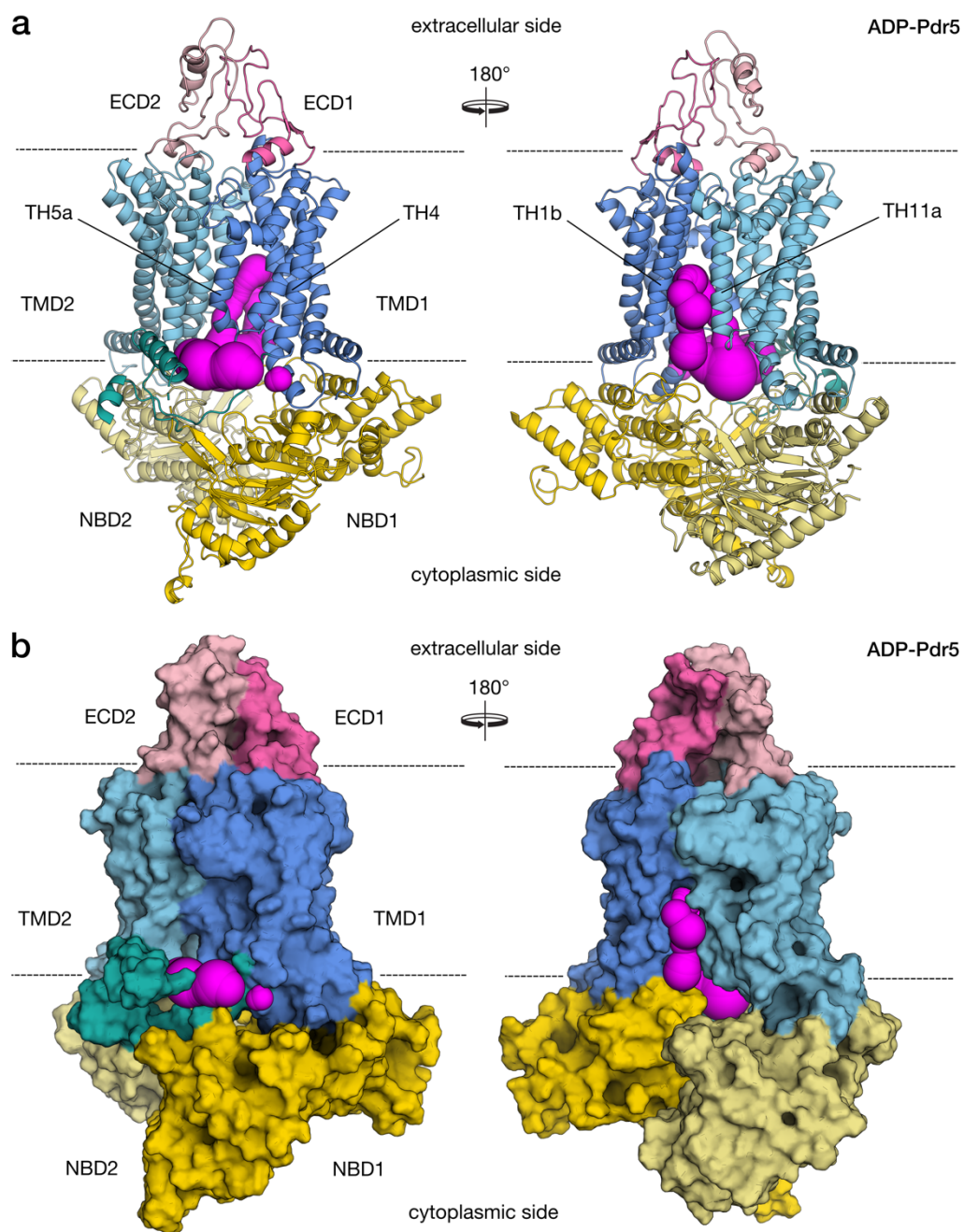
Supplementary Figure 8. ATPase activity of Pdr5 linker domain mutants in plasma membrane vesicles. **a** Coomassie-stained SDS-PAGE (single repeat) of plasma membrane vesicles containing wild-type Pdr5 and mutants in the linker domain (LD). The signals of Pdr5 and Pma1 (normalisation standard) are indicated with arrows. Densitometric analysis (Fiji) indicated differences in expression levels below 10%. The same result was obtained when taking the signal intensity of Pma1 into account. Therefore, no expression level correction was applied. **b** ATPase activity of Pdr5 reconstituted in plasma membrane vesicles. Shown are the kinetic curves for the ATP hydrolysis by wild-type protein and linker domain mutants. The experiment was performed using $n=3$ biologically independent samples examined over 3 independent experiments. Error bars in figure represent mean \pm standard error. See also: Supplementary Table 4. Source data are provided as a Source Data file.



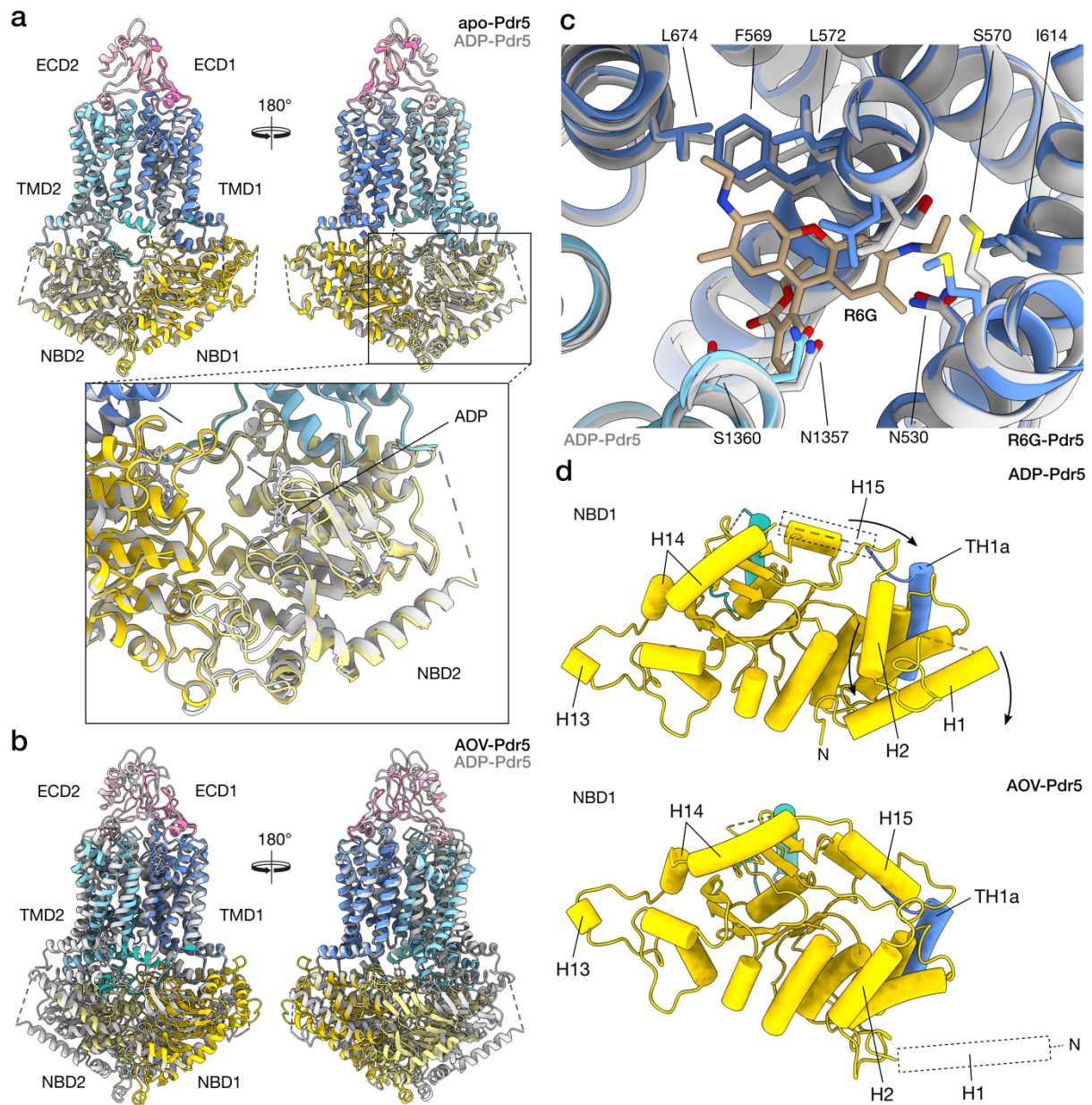
Supplementary Figure 9. Glycosylation of Pdr5. Figure shows the side view of the Pdr5 and, in inset, a putative glycosylation site on the extracellular domain of Pdr5. The two transparent surface representations of the apical portion of Pdr5 are from the same ADP-Pdr5 cryo-EM map, contoured at two different levels. The inner surface shows the Coulomb potential map immediately surrounding the protein; the outer is a noisier and Gaussian-filtered (2σ) version of the map, showing the protrusion around the asparagine residue (labelled), previously suggested to be glycosylated. Abbreviations: ECD, extracellular domain; TMD, transmembrane domain.



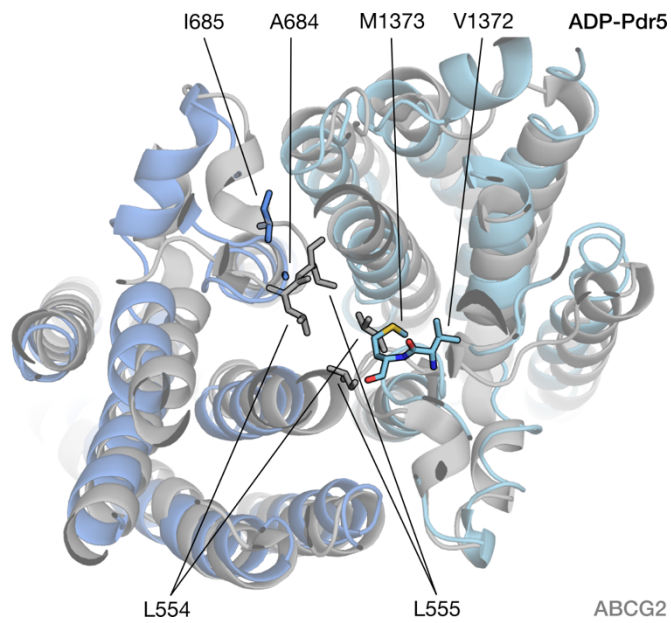
Supplementary Figure 10. Details of protein-ligand interactions in Pdr5. Schematic representation of the network of molecular interactions between the nucleotides and the protein in the canonical and inactive nucleotide-binding sites of the **a** inward-facing ADP-Pdr5 and **b** the outward-facing AOV-Pdr5. The interactions between the transport substrate rhodamine 6G and the residues in the **c** substrate entry channel in the inward-facing R6G-Pdr5 are similarly depicted. Also shown is the superposition of cartoon models of R6G-Pdr5 and human multi-drug transporter ABCG2 (pink, PDB-ID: 6VXI) in complex with **d** the chemotherapy drug mitoxantrone. Interaction diagrams were prepared with LigPlot+². Atoms are depicted as coloured balls (C, black; N, blue; O, red; P, purple; S, yellow; Mg, V, green), ligand covalent bonds are purple and protein bonds are brown. Dashed green lines represent hydrogen bonds or other electrostatic interactions, with inter-atom distances indicated in Å. The radiating arc symbol represents amino-acid residues involved in hydrophobic contacts. Abbreviations: MIX, mitoxantrone; R6G, rhodamine 6G.



Supplementary Figure 11. Analysis of potential entry sites in the inward-facing conformation of Pdr5. **a** Cartoon representation of the inward-facing state and the present tunnels (magenta) as determined by CAVER-3.0³. **b** Surface representation of Pdr5. This analysis demonstrates that Pdr5 has only one membrane entry site between helices TH1b and TH11a, while the corresponding entrance on the opposite side is closed by TH4 and TH5a. The position of the membrane is indicated by dashed black lines.



Supplementary Figure 12. Structural differences between Pdr5 models. Shown here are structural overlays of Pdr5 models in cartoon representation: **a**) between apo-Pdr5 and ADP-Pdr5, with the inset showing details of the NBD2 domain around the catalytic NBS; **b**) AOV-Pdr5 and ADP-Pdr5 (or outward-facing and inward-facing conformations); **c**) between R6G-Pdr5 and ADP-Pdr5 in the region surrounding the rhodamine 6G transport substrate. In panels **a–c**, ADP-Pdr5 structure is used as a reference and is coloured grey. Other models follow the domain colouring scheme used elsewhere in the paper. **d**) The diagram depicts the difference between the conformation of NBD1 domain of Pdr5 in outward- and inward-facing models (ADP-Pdr5 and AOV-Pdr5). In ADP-Pdr5, the N-terminal helices H1 and H2 are clearly resolved in the cryo-EM map, unlike helix H15, which did not adopt a discrete conformation. In AOV-Pdr5, H15 moves towards transmembrane helix TH1a, displacing H2 and H1, the latter of which is no longer visible in the map. Dashed lines denote the approximate position of unresolved helices, and arrows are an indication of movement. Abbreviations: ECD, extracellular domain; NBD, nucleotide-binding domain; R6G, rhodamine 6G; TMD, transmembrane domain.



Supplementary Figure 13. Leucine gate of human ABCG2 and the corresponding region of Pdr5. Human ABCG2 (grey, PDB-ID: 6HCO [<http://doi.org/10.2210/pdb6HCO/pdb>]) and Pdr5 (coloured) were superimposed and the residues of ABCG2 forming the di-leucine gate (L554 and L555) are highlighted (ABCG is a homodimer). The corresponding residues of Pdr5 (A684/I685 and V1372/M1373) are also highlighted.

Supplementary Tables

Supplementary Table 1. Cryo-EM data collection and refinement statistics

Protein structure	apo-Pdr5	ADP-Pdr5	R6G-Pdr5	AOV-Pdr5
Organism	<i>S. cerevisiae</i>	<i>S. cerevisiae</i>	<i>S. cerevisiae</i>	<i>S. cerevisiae</i>
PDB ID	7P03	7P04	7P05	7P06
EMDB ID	EMD-13142	EMD-13143	EMD-13144	EMD-13145
Data collection				
Microscope	FEI Titan Krios	FEI Titan Krios	FEI Titan Krios	FEI Titan Krios
Voltage (kV)	300	300	300	300
Detector	K2 Summit	K3	K3	K3
Mode	counting	counting, super-resolution	counting, super-resolution	counting, super-resolution
Nominal magnification	130,000 ×	130,000 ×	130,000 ×	130,000 ×
Pixel size (Å/pix)	1.07	0.326	0.326	0.326
Electron fluency, per frame (e ⁻ /Å ²)	1.452	0.96	0.97	0.98
Electron fluency, total (e ⁻ /Å ²)	58.1	47.21	47.73	48.13
Defocus range (µm), step (µm)	-0.8 to -2.7, 0.3	-0.7 to -2.2, 0.3	-0.7 to -2.2, 0.3	-0.7 to -2.2, 0.3
Exposure (s)	12	1.31	1.31	1.31
Frames	40	49	49	49
Number of micrographs	4,211	3,415	3,604	8,370
Reconstruction				
Software	RELION-3.0 / cryoSPARC-2.15	RELION-3.1	RELION-3.1	RELION-3.1 / cryoSPARC-3.0
Final number of particle images	68,154	95,283	76,419	55,155
Est. translational accuracy (pix)	–	0.427	0.643	–
Est. rotational accuracy (°)	–	1.136	1.669	–
Map resolution, FSC _{0.143} (Å)	3.45	2.85	3.13	3.75
Map-sharpening B factor (Å ²)	-102.9	-47.4	-55.0	-83.3
Model composition				
Non-hydrogen atoms	21,163	21,583	21,645	21,533
Protein residues	1,333	1,353	1,353	1,350
Ligands (PDB)	–	1 × ATP 1 × ADP	1 × ATP 1 × ADP 1 × R6G	1 × ATP 1 × AOV 1 × MG
Refinement				
Software	Phenix-1.18.2	Phenix-1.18.2	Phenix-1.18.2	Phenix-1.18.2
Correlation coefficient, masked	0.80	0.81	0.82	0.79
Correlation coefficient, box	0.67	0.60	0.66	0.52
Model resolution, FSC _{0.5} (Å)	3.7	3.0	3.3	3.6
Validation (proteins)				
MolProbity score	1.71	1.62	1.67	1.91
Clash score, all atoms	6.14	7.14	7.16	9.39
EMRinger score	3.09	–	–	–
Ramachandran plot statistics				
Favoured, overall (%)	94.63	96.5	95.97	93.82
Allowed, overall (%)	5.37	3.5	4.03	6.81
Outlier, overall (%)	0.06	0	0	0
R.m.s. deviations				
Bond length (Å)	0.006	0.073	0.006	0.006
Bond angle (°)	0.678	0.711	0.551	0.703

Supplementary Table 2. Structural alignment of Pdr5 and related proteins.

Transporter	PDB-ID	R.m.s.d. vs. Pdr5 IF* [Å]	R.m.s.d. vs. Pdr5 OF** [Å]
TarGH	6jbh	14 (359)	13.9 (358)
Wmz-Wzt / ATP	6m96	9.2 (343)	8.8 (338)
Wmz-Wzt / ATP-Mg ²⁺	7k2t	13.4 (727)	10.5 (667)
ABCA1	5xjy	33.3 (762)	36.3 (808)
ABGG2 OF**	6hbu	5.1 (1006)	2.8 (881)
ABCG2 IF*	6hco	3.9 (929)	6.8 (988)
ABCG5/G8	5do7	4.3 (753)	6.6 (821)

Note: R.m.s.d. calculation considered only backbone atoms and was carried out in PyMOL (Schrödinger LLC). Numbers in parentheses indicate residue range of alignment. *: inward-facing; **: outward-facing.

Supplementary Table 3. Summary of the statistical analysis of the liquid drug assays.

Mutation	Drug			
	R6G	FC	KC	CH
Q801A	0.9976 (ns)	0.9817 (ns)	0.7321 (ns)	<0.0001 (****)
Q801V	0.9924 (ns)	<0.0001 (****)	0.9212 (ns)	<0.0001 (****)
K802A	0.9226 (ns)	<0.0001 (****)	0.1629 (ns)	0.0002 (***)
K802E	0.9968 (ns)	0.0032 (**)	0.0015 (**)	<0.0001 (****)
G803A	0.9998 (ns)	0.0468 (*)	0.8752 (ns)	0.9998 (ns)
G803V	0.2768 (ns)	0.9927 (ns)	0.9931 (ns)	0.4863 (ns)
E804A	0.0036 (**)	<0.0001 (****)	0.9974 (ns)	0.9112 (ns)
I805S	0.9998 (ns)	0.9994 (ns)	0.0002 (***)	<0.0001 (****)

Note: Analysis was carried out using a one-way ANOVA test in Prism 9 (GraphPad Inc.). ****: $p < 0.0001$, ***: $p < 0.0005$, **: $p < 0.005$, *: $p < 0.5$, not significant (ns): $p > 0.5$. See also: Supplementary Figure 7. Abbreviations: R6G, rhodamine 6G; FC, fluconazole; KC, ketoconazole; CH, cycloheximide.

Supplementary Table 4. Summary of the kinetic parameters of the ATPase activity of wild-type Pdr5 and the mutants of the linker domain.

Mutation	K_M [mM]	V_{max} [$\mu\text{mol min}^{-1} \text{mg}^{-1}$]	Difference with wild type	
			K_M	V_{max}
Wild type	1.7 ± 0.2	3.2 ± 0.1	–	–
Q801A	1.1 ± 0.4	1.7 ± 0.2	0.5913 (ns)	<0.0001 (****)
Q801V	2.0 ± 0.3	1.6 ± 0.1	0.98 (ns)	<0.0001 (****)
K802A	0.9 ± 0.2	0.8 ± 0.1	0.2786 (ns)	<0.0001 (****)
K802E	1.3 ± 0.2	1.7 ± 0.1	0.9078 (ns)	<0.0001 (****)
G803A	0.7 ± 0.1	1.1 ± 0.1	0.1016 (ns)	<0.0001 (****)
G803V	1.6 ± 0.4	1.2 ± 0.1	0.9997 (ns)	<0.0001 (****)
E804A	2.3 ± 0.4	1.2 ± 0.1	0.5913 (ns)	<0.0001 (****)
I805S	1.7 ± 0.3	3.2 ± 0.2	>0.9999 (ns)	>0.9999 (ns)

Note: Statistical analysis was carried out using a one-way ANOVA test (Prism 9, GraphPad Inc.) and revealed no significant differences (ns) in K_M , but highly significant differences for seven of the eight mutants (****, $p < 0.0001$). Errors report standard deviation of at least three independent experiments.

Supplementary Table 5. Selected mutations of Pdr5 with functional impact and possible structural explanation of the observed functional modulation of Pdr5.

Mutation	Location	Modulation of Pdr5 function	Reference	Explanation based on the structures
E244G	Q-loop of NBD1	Increased drug sensitivity	⁴	Interaction with D-loop of NBD1
T257I	H6	Alters drug specificity	Uniprot P33302	Not evident
G302D	Loop preceding the C-loop of NBD1 (X-loop)	Generalized drug resistance	Uniprot P33302	Stabilizes the conformation of the C-loop of NBD1
S558Y	TH2	Impaired transport activity	⁵	Interacts with the linker TH11a-TH11b
S648F	TH4	Alters drug specificity	Uniprot P33302	Forms a helical bundle with TH5c and TH6
G905S	Walker A of NBD2	Inactivates transport	Uniprot P33302	ATP binding / hydrolysis
G908S	Walker A of NBD2	Inactivates transport	Uniprot P33302	ATP binding / hydrolysis
Q951G	Q-loop of NBD2	Increased drug sensitivity	⁴	ATP binding / hydrolysis
G1009C	Loop preceding the C-loop of NBD2 (X-loop)	Generalized drug resistance	Uniprot P33302	Interaction with LD1 (QKGE[L])
G1040D	D-loop of NBD2	Alters drug specificity	Uniprot P33302	Impaired NBD-NBD communication
D1042N	D-loop of NBD2	Alters drug specificity	⁶	Impaired NBD-NBD communication
S1048V	H23	Alters drug specificity	Uniprot P33302	Not evident
Y1311S	TH9b	Alters drug specificity	Uniprot P33302	Cluster of Y residues (1301, 1305, 1306, 1311)
S1360F	TH11a	Alters drug specificity	⁷	Part of the R6G binding site
S1386A	TH11a	Creates bi-directional transport	⁸	On top of the R6G binding site
T1393I	TH11c	Alters drug specificity	Uniprot P33302	On top of the R6G binding site

Note: The multiple suppressor mutants of Pdr5, which have been described in the literature (see, for example^{4,9}), have been excluded due to potential additive effects that cannot be predicted from the wild-type structure.

Supplementary References

1. Lamping, E. *et al.* Fungal PDR transporters: Phylogeny, topology, motifs and function. *Fungal Genetics and Biology* **47**, 127–142 (2010).
2. Laskowski, R. A. & Swindells, M. B. LigPlot+: Multiple Ligand–Protein Interaction Diagrams for Drug Discovery. *J. Chem. Inf. Model.* **51**, 2778–2786 (2011).
3. Chovancova, E. *et al.* CAVER 3.0: a tool for the analysis of transport pathways in dynamic protein structures. *PLoS Comput Biol* **8**, e1002708 (2012).
4. Ananthaswamy, N. *et al.* The signaling interface of the yeast multidrug transporter Pdr5 adopts a cis conformation, and there are functional overlap and equivalence of the deviant and canonical Q-loop residues. *Biochemistry* **49**, 4440–4449 (2010).
5. Sauna, Z. E. *et al.* Mutations Define Cross-talk between the N-terminal Nucleotide-binding Domain and Transmembrane Helix-2 of the Yeast Multidrug Transporter Pdr5. *J Biol Chem* **283**, 35010–35022 (2008).
6. Furman, C. *et al.* The Deviant ATP-binding Site of the Multidrug Efflux Pump Pdr5 Plays an Active Role in the Transport Cycle. *J. Biol. Chem.* **288**, 30420–30431 (2013).
7. Kueppers, P., Gupta, R. P., Stindt, J., Smits, S. H. J. & Schmitt, L. Functional Impact of a Single Mutation within the Transmembrane Domain of the Multidrug ABC Transporter Pdr5. *Biochemistry* **52**, 2184–2195 (2013).
8. Mehla, J. *et al.* Evidence for a molecular diode-based mechanism in a multispecific ATP-binding cassette (ABC) exporter: SER-1368 as a gatekeeping residue in the yeast multidrug transporter Pdr5. *J Biol Chem* **289**, 26597–26606 (2014).
9. Downes, M. T. *et al.* The Transmission Interface of the *Saccharomyces cerevisiae* Multidrug Transporter Pdr5: Val-656 Located in Intracellular Loop 2 Plays a Major Role in Drug Resistance. *Antimicrob Agents Chemother* **57**, 1025–1034 (2013).